



Effect of double aging on mechanical properties and microstructure of EV31A alloy

Kan GU^{1,2}, Xiao-qin ZENG^{1,2}, Bin CHEN¹, Ying-xin WANG^{1,2}

1. School of Materials Science and Engineering, Shanghai Jiao Tong University, Shanghai 200240, China;

2. National Engineering Research Center of Light Alloy Net Forming and State Key Laboratory of Metal Matrix Composite, Shanghai Jiao Tong University, Shanghai 200240, China

Received 6 November 2020; accepted 20 May 2021

Abstract: To improve the ductility of a commercial Mg–rare earth alloy EV31A (Mg–3Nd–1.5Gd–0.3Zn–0.5Zr), a heat treatment method called double aging is explored, and its effect on mechanical properties and microstructure of the alloy is studied. Ultimate strength and elongation of the alloy can be increased to 288 MPa and 6.6% by the optimum double aging process, compared to 273 MPa and 4.9% after single aging. Time consumption of the aging process is also significantly decreased from 16 h (single aging) to 2 h. HAADF-STEM characterization shows that the primary precipitate is β' phase, which is similar to β' phase in Mg–Nd binary alloy. By double aging, the β' phase is finer and more densely distributed compared with single aging, with approximately double density and half size, which explains the improvement in strength and ductility.

Key words: magnesium alloy; EV31A; double aging; mechanical properties; β' phase

1 Introduction

Due to its low density and high specific strength, magnesium alloy has aroused widespread interest in various industry fields, including automobile and aerospace. However, low strength and poor ductility have limited further application of magnesium alloy. To improve the mechanical properties of Mg alloys, alloying with rare earth (RE) elements is adopted as one of the most effective ways. Not only can RE addition strengthen the alloy by solid solution strengthening and precipitation strengthening with hard eutectic phases [1,2], but it can also improve the ductility by weakening the texture [3,4]. Therefore, a lot of efforts have been made on developing high strength Mg–RE alloys [5–7]. Except for tuning the composition by alloying, control of the age

hardening process is also important for improving mechanical properties, since most of the Mg–RE alloys have good age hardening responses [8].

Currently, double aging has been explored as a subtler and more efficient aging technique. Previous researches on double aging were usually focused on light alloys, including Mg–Zn alloys [9–12], Al alloys [13–16], and other alloy systems [17,18]. But few studies have been made for double aging of Mg–RE alloys. Generally speaking, double aging is a two-step aging process following a “low–high” pattern. The first step, also called pre-aging, usually uses a temperature lower than that in the single aging process, while the second step (second aging) uses a higher temperature. But there are also very few exceptions that follow “high–low” patterns [18]. Effects of double aging vary in different alloy systems, but in most cases, double aging is found to make the precipitates finer and increase the strength

of the alloy, with less time consumption compared to the single aging process [9–14]. In this work, finer and evenly distributed G.P. zone will be prepared by low-temperature pre-aging, and then precipitation process can be accelerated by high-temperature second aging, improving mechanical properties and consuming less time.

To have some insight into the effect of double aging on Mg–RE alloy, EV31A alloy has been chosen as the research subject. EV31A, also called Elektron 21, has a theoretical composition of Mg–3Nd–1.5Gd–0.3Zn–0.5Zr. This alloy is widely used in the non-conventional manufacturing and aerospace industry for its excellent mechanical properties, good workability, and outstanding anti-corrosion properties [19]. Though EV31A has better strength compared to other common commercial Mg–RE alloys, its ductility is relatively poor [19]. So, hopefully, by using double aging, the ductility of EV31A and efficiency of heat treatment can be improved without sacrificing strength, which is favorable in industrial applications. As for the aging process, though the precipitation sequences of binary Mg–Nd [20] and Mg–Gd [21] have been determined as

Mg–Nd: SSSS→G.P. zone→ β' (cbco)→ β (bct)

Mg–Gd: SSSS→ β'' (D0₁₉)→ β' (cbco)→ β_1 (fcc)

There has not been a decisive conclusion on the precipitation sequence of such Mg–Gd–Nd alloy as EV31A. KIELBUS et al [22,23] claimed that the precipitation sequence of EV31A is SSSS→ β'' (D0₁₉)→ β' (cbco)→ β_1 (fcc), while RIONTINO et al [24] suggested SSSS→ β'' →(β')→ β_1/β , in which the existence of β' phase is only supported by positron annihilation spectroscopy. GILL et al [25] suggested SSSS→ β'' (D0₁₉)→ β' (fcc) for a similar Mg–3Nd–2Gd alloy, but fcc-structured β' phase has not been reported elsewhere in Mg–Nd and Mg–Gd binary alloys. No matter what theory is taken, it is certain that the major strengthening phase of EV31A alloy is β' phase. Characterization of precipitate phase is the indispensable basis for understanding the strengthening mechanism, so it will be an important part of this research.

In this work, different parameters of double aging are evaluated to find the optimum parameter for EV31A alloy. Then, the effect and efficiency of double aging will be compared to single aging. Besides, the precipitate phases in EV31A alloy will

be characterized, and the microstructure of single and double aged alloy will be compared to find the mechanism of double aging.

2 Experimental

An alloy with a nominal composition of Mg–3Nd–1.5Gd–0.3Zn–0.5Zr was prepared by induction heating under argon gas protection. The actual composition of the alloy was determined to be Mg–3.07Nd–1.40Gd–0.29Zn–0.6Zr. The sample was solutionized at 520 °C for 8 h, and then water-quenched. To determine the optimum aging parameter, single aging and double aging at different temperatures for different time were carried out. Vickers hardness tests were carried out at a load of 2500 g for 10 s (AolongXingdi HV–30). Each data point is averaged from 10 tests. For single aging, samples aged at 175, 200, and 225 °C were tested. For double aging, samples aged at 125, 150, and 175 °C for 0.5, 1, 2, and 4 h pre-aging were tested. For each set of pre-aging parameters, 200 and 225 °C second aging were also compared. Tensile tests were carried out to get more exact results, in which differently aged (with parameters similar to hardness test) dog-bone-shaped specimens shown in Fig. 1 were tested with the cross-head speed of 2 mm/min, with 2 tests for each data point (Zwick/Roell Z100).

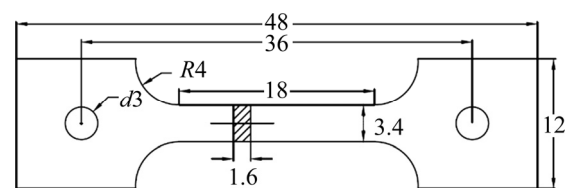


Fig. 1 Specification of tensile specimen (mm)

Specimens for optical microscopy were prepared by grinding, polishing and etching with 4% nitric acid–ethanol solution, and observed by Axio Observer A1. Specimens for TEM were prepared by cutting $d3$ mm discs, mechanical thinning to $<100 \mu\text{m}$, double-jet electro-polishing with 3% perchloric acid at $-40 \text{ }^\circ\text{C}$, and ion-milling by GATAN PIPS II for 20 min at $1.5 \text{ keV}/\pm 2^\circ$. HAADF-STEM images were taken by Talos F200X G2 (for single aged samples) and Talos F200X (for double aged samples), by which EDS analysis was also carried out.

3 Results and discussion

3.1 Effect of double aging on mechanical properties of EV31A

Hardness variation of EV31A alloy at 175, 200, and 225 °C single aging is shown in Fig. 2. Before aging, the samples have been solutionized, with their hardness at around HV 54. All the aging curves show one single peak, and there is no sign of a second peak till 200 h. Aging at 225 °C steeply increases the hardness of the alloy, during which the hardness of the sample has reached HV 77 after only 0.5 h, and then reached HV 81 (peak) after 2 h. As for the aging process at 200 and 175 °C, a mild increase of hardness with increasing aging time is shown, and the peak hardness is HV 83 (at 16 h), and HV 84 (at 200 h), respectively. Taking both performance and efficiency into consideration, 200 °C and 16 h are determined as the optimum single aging parameters. Though peak hardness at 175 °C is a little bit higher, aging time above 100 h is too costly for manufacturing. In the following tests, samples after 200 °C, 16 h single aging will serve as a benchmark to evaluate the effect of double aging.

Vickers hardness variation of EV31A alloy

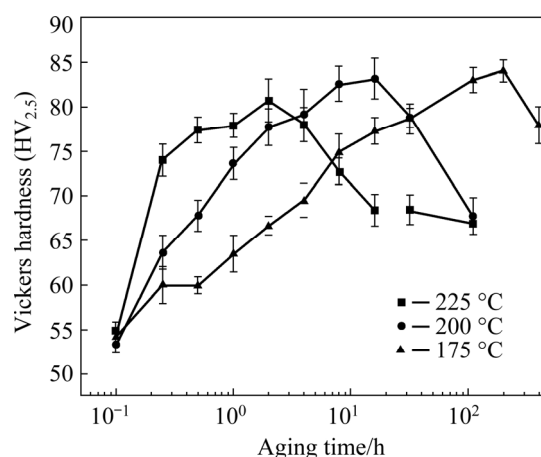


Fig. 2 Vickers hardness of EV31A alloy after solutionization at 175, 200 and 225 °C single aging versus aging time

during different double-aging processes is shown in Fig. 3. Six sets of pre-aging temperature–time combinations are tested, including 0.5 and 1 h at 175 °C, 1 and 2 h at 150 °C, and 2 and 4 h at 125 °C. Such design is intended to cover the incubation period of the primary phase at a lower temperature, which, in theory, will make the precipitate phase finer, improving the mechanical properties of the alloy. Since there is no previous research on the incubation period of EV31A or

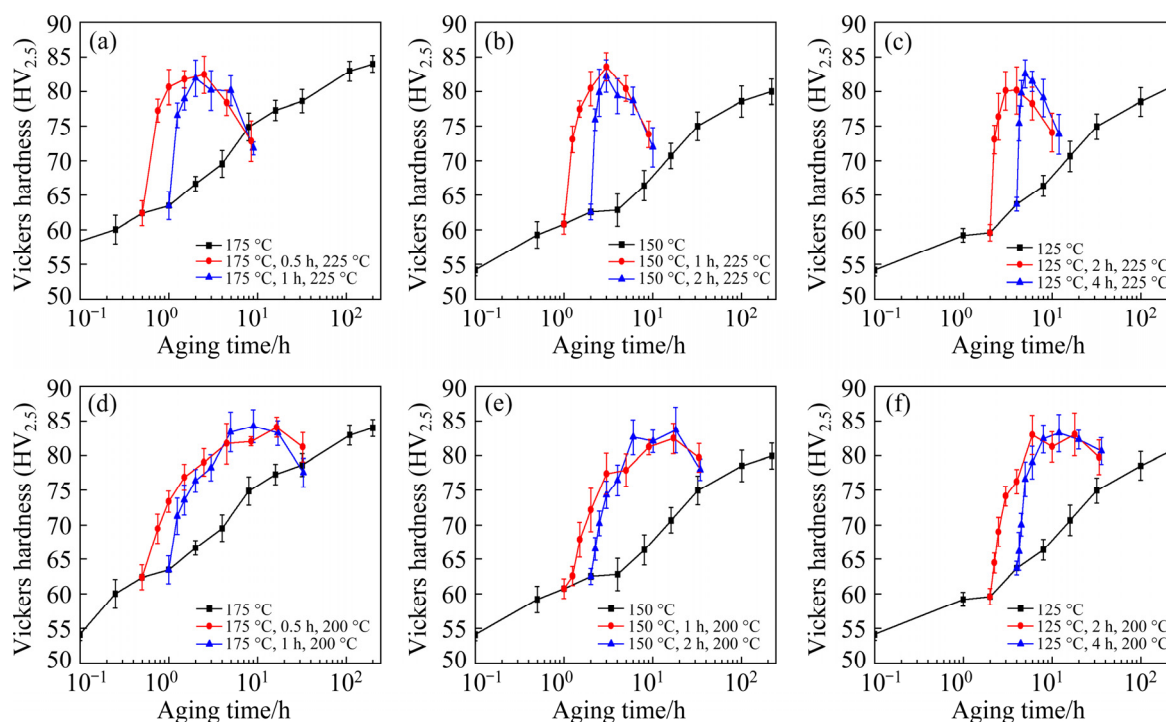


Fig. 3 Vickers hardness of EV31A alloy after solutionization during double aging with pre-aging temperature set at 175 °C (a, d), 150 °C (b, e) and 125 °C (c, f), and second aging temperature set at 225 °C (a–c) and 200 °C (d–f)

Mg–Nd–Gd alloy, the experiment design refers to the time–temperature–transformation (TTT) curve of Mg–Nd alloy calculated by PIKE and NOBLE [26]. For second-aging, samples aged at two different second-aging temperatures, 200 and 225 °C, are tested after each set of pre-aging to find the best temperature and peak aging time. It is shown in Fig. 3 that the peak hardness for almost all the combinations of double aging parameters reaches HV 82–84. So, considering the limited precision of the hardness test, it is too early to determine the best combination directly from it. However, several conclusions can be drawn: (1) The effect of double aging is, at least, not worse than the effect of single aging. The 200 °C, 16 h single aged sample shows peak hardness of HV 83, which is close to that of the double aged sample. (2) The difference in peak hardness with different second-aging temperatures is quite small, while the second-aging time is significantly decreased at higher temperatures. At 200 °C, it takes 8–16 h for second-aging to reach peak hardness, which is close to what is observed in the single-aging test. However, at 225 °C, only 1–2 h is needed for peak aging, which is already short enough, excluding the necessity of testing even higher second-aging temperatures. Since at 225 °C, aging time can be greatly saved without sacrificing mechanical properties, parameters for second-aging can be determined as 225 °C, 1 h.

Since the optimum pre-aging parameter remains unknown due to the precision limitation of the hardness test, tensile tests are carried out to provide more information on the effect of pre-aging parameters. Ultimate tensile strength (UTS) and elongation of samples with different pre-aging parameters are shown in Fig. 4(a), while second-aging parameters are fixed at 225 °C, 1 h. It is shown that pre-aging at 175 °C for 1 h shows the best effect on both UTS and elongation, which reach 288 MPa and 6.6%, respectively. Thus, the optimum parameter for the whole double aging process can be determined as 175 °C, 1 h + 225 °C, 1 h.

Moreover, with pre-aging temperature fixed, both UTS and elongation seem to have an increase–decrease transition with increasing pre-aging time. This phenomenon may be caused by Guinier–Preston (G.P.) zone formed in the pre-aging period, which will be proven by the

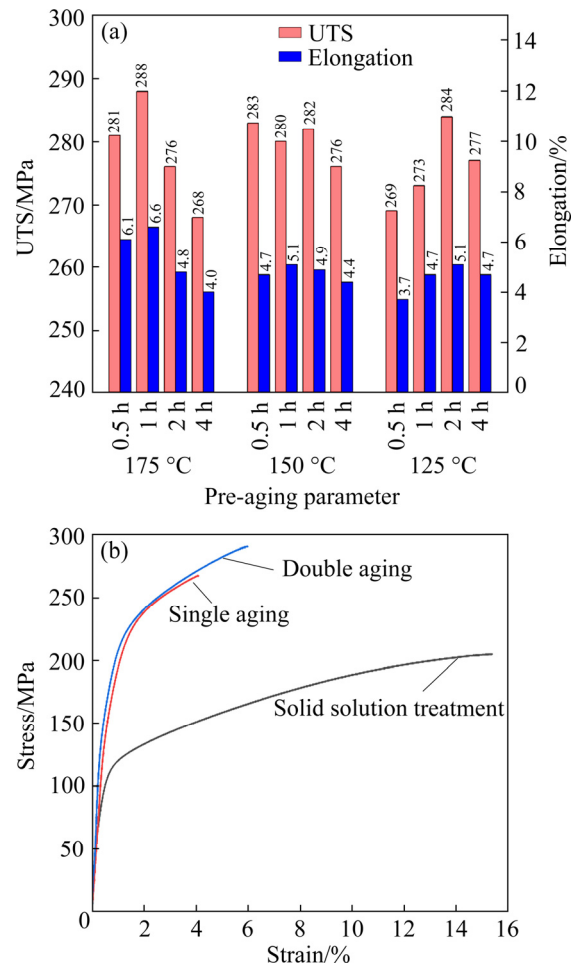


Fig. 4 Ultimate tensile strength (UTS) and elongation of samples with different pre-aging parameters and second-aging at 225 °C for 1 h (a) and stress–strain curves of samples after solid solution treatment, single aging (200 °C, 16 h) and double aging (175 °C, 1 h + 225 °C, 1 h) (b)

HAADF-STEM characterization later. If the pre-aging time is too short, the formation of G.P. zone is far from complete, and most of nucleation remains to take place in the second-aging process, which makes no difference from single aging. If the pre-aging time is too long, β' phases start to grow, absorbing excess G.P. zones and decreasing the number of nucleation sites for β' phases. Only around the exact point when the most amount of G.P. zone is formed, there will be most nucleation sites for β' phases. Then, by second-aging, maximum amount of fine, densely distributed β' phases can grow, contributing to the mechanical properties of the alloy. Also, it is shown that the optimum pre-aging time tends to be longer with lower pre-aging temperature, which is 1 h for

175 °C and 2 h for 125 °C. Though for 150 °C, the optimum time is not very clear due to the potential inaccuracy of tensile tests, it is speculated to be 1–2 h. The ideal target of the pre-aging process is, in theory, the formation of the G.P. zone to the maximum amount, which is probably the case at the optimum time mentioned above.

The stress–strain curves for the solutionized sample, the single aged sample, and the double aged sample with optimum parameter are compared in Fig. 4(b). For UTS and elongation, the solutionized sample shows 201 MPa and 14.7%, and the single aged sample shows 273 MPa and 4.9%, respectively. Though both the stress–strain curves of single and double aging show typical features of plastic fracture, the double aged sample shows better strength and ductility (288 MPa and 6.6%). This is because β' phases are finer and more densely distributed with double aging. They strengthen the alloy in two ways. First, the double aged sample shows a little higher yield strength, attributed to Orowan strengthening [27]. More importantly, refined and dense β' phases can inhibit dislocation movements better, explaining the significant improvement in work hardening response during plastic deformation. The

improvement in ductility can be explained by more evenly distributed β' phases weakening the tendency of fracture.

3.2 Effect of double aging on microstructure of EV31A alloy

Images from optical microscopy of EV31A alloy after solid solution treatment, pre-aging, single and double aging are shown in Fig. 5. Since there is no deformation processing adopted, the grain size of the alloy is quite large (200–500 μm), and most of the grains are equiaxed. Besides, there is no significant change in grain size before and after the aging process, indicating that the primary strengthening mechanism is precipitation instead of grain size reduction, which is natural given the relatively low temperature of the whole aging process.

It is worth noticing that there are some black round “dots” with $\sim 50 \mu\text{m}$ in diameter in Fig. 5, which are clustered precipitates distributing mainly inside the grains. They are also observed by HAADF-STEM, as shown in Fig. 6(a). There are two kinds of precipitates in the cluster. One of them is darker (lower contrast) rods or ellipsoids, which are 1–2 μm in length and 50–100 nm in diameter.

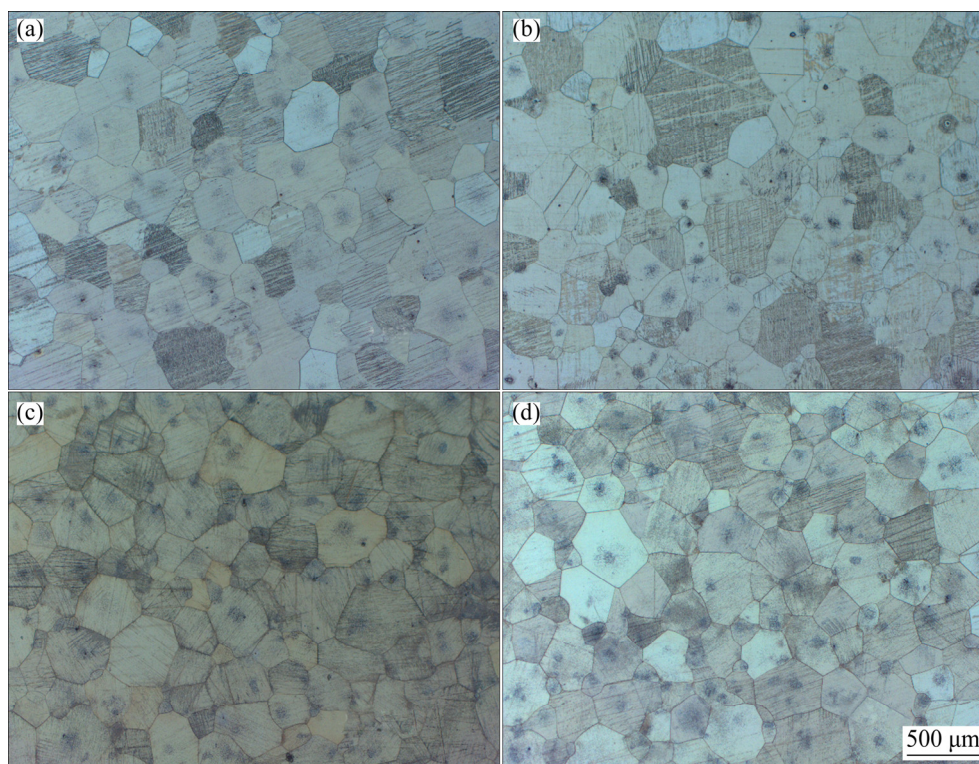


Fig. 5 Images from optical microscopy of EV31A alloy after solid solution treatment (520 °C, 8 h) (a), pre-aging (175 °C, 1 h) (b), single aging (200 °C, 16 h) (c), and double aging (175 °C, 1 h + 225 °C, 1 h) (d)

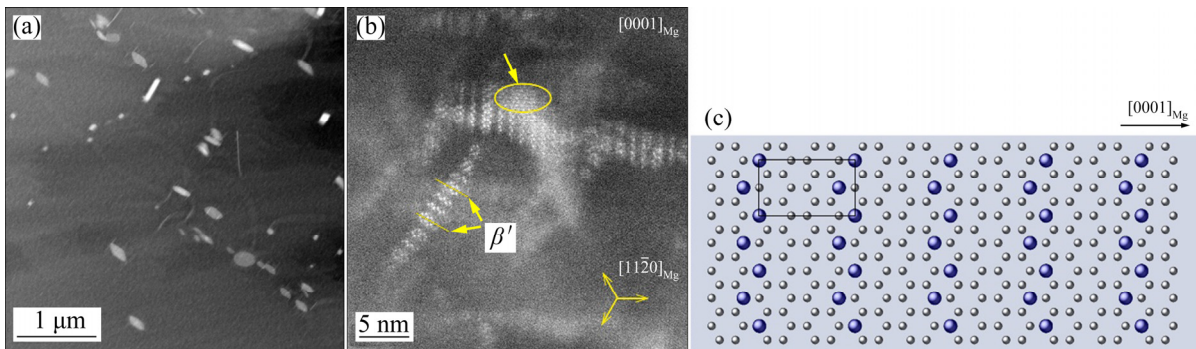


Fig. 6 HAADF-STEM images of clusters of Mg–Zr (dark) and Mg–Zn–Zr (bright) precipitates (a) and β' precipitates (b) in single aged sample (200 °C, 16 h) and illustration of structure of β' phases (c) in EV31A

Another one is brighter (higher contrast) rods, which are 100–500 nm in length and 50–100 nm in diameter. EDS analysis shows that the dark rods contain only Mg and Zr, while the brighter ones contain Mg, Zr and Zn. The higher contrast of Mg–Zr–Zn precipitate is probably due to its higher content of alloying elements. Previous research shows that a low level of Zn addition can alter the aging response of the alloy, and Zr addition has a potential grain refining effect [19], which indicates that these minor phases may have some subsidiary strengthening effects. It is worth noticing that these phases are observed in only a few areas of the alloy, and thus should not be regarded as primary precipitation phases. Considering both element composition and amount of precipitation phases, the primary strengthening phase of the alloy should still be the Mg–RE β' phase, though it is too small to be observed directly by optical microscope.

Figure 6(b) shows the HAADF-STEM image of β' precipitates in a single aged sample. β' precipitates in the single aged alloy are stripe-shaped, about 10–50 nm in length and 5–10 nm in width, extending along $\langle 11\bar{2}0 \rangle_{\text{Mg}}$ direction. The orientation relationships are $(100)_{\beta'} // \langle 11\bar{2}0 \rangle_{\text{Mg}}$ and $(001)_{\beta'} // (0001)_{\text{Mg}}$. β' precipitates in EV31A show very weak contrast under incident beam along other directions, especially $\langle 11\bar{2}0 \rangle_{\text{Mg}}$ direction, which indicates that such stripe may be very thin in $[0001]_{\text{Mg}}$ direction. β' phases in EV31A contain zigzag chains and hexagonal rings of RE atom aligned in rows, which is similar to β' phases found in Mg–Nd binary alloy [20]. The unit cell of β' phases is orthorhombic with lattice constants of $a=a_0=0.64$ nm, $b=2\sqrt{3}a_0=1.14$ nm, $c=c_0=0.52$ nm and atomic ratio of Mg:RE. Such structure is also

known as β' -short, which usually found in Mg–Nd alloy. In contrast, there is another β' -long structure with $b=4\sqrt{3}a_0$, which is usually found in Mg–Gd alloy. Basic structure of β' -short contains only zigzag chains, and the hexagonal rings shown in Fig. 6(b) are the result of β' units joining in an upside-down style. One typical β' unit is marked out in Fig. 6(b). The similar microstructure of β' phase between EV31A and Mg–Nd alloy is expected, since amount of Nd atoms in EV31A is about twice as much as Gd atoms. This similarity is also supported by EDS analysis. It is shown that β' precipitates in EV31A have 4.21 at.% Nd and 1.12 at.% Gd, with Nd/Gd ratio close to 4, which is much higher than 2 from the whole alloy composition. For comparison, Mg matrix contains 1.96 at.% Nd and 0.79 at.% Gd, with Nd/Gd ratio close to 2. ISSA et al [28,29] used first-principle calculations and found that β' structures of different Mg–RE alloys are closely related to the interfacial energy of Mg/ β'' prismatic interfaces. Since β' phase in EV31A contains more Nd than Gd, the interfacial energy will be close to that of β' phase in Mg–Nd binary alloy, thus showing similar structures with the lowest energy. There is also an area with a different crystal structure besides the β' phase, which is circled out in Fig. 6(b). Different from β' structure, RE atoms in this area seem to have an unusual hexagonal alignment, which is similar to the quasi- β_1 structure that TAN et al [30] found in Mg–Nd alloy. It is explained that such structure is similar to the β_1 structure projected along $\langle 111 \rangle$ zone axis, and is probably transformed from two β' units inserted into each other in an in-situ manner.

HAADF-STEM images of β' phases in the

single aged sample and the double aged sample are shown in Fig. 7. Under the same magnification, it is clearly shown that β' phases in the double aged sample are finer and more densely distributed. Compared to β' phases in the single aged sample, which are 10–50 nm in length and 5–10 nm in width, β' phases in the double aged sample are only 5–20 nm in length and 2–5 nm in width. The precipitation density of both samples cannot be precisely estimated by the HAADF-STEM images since they contain β' phases at different depths, but a rough count shows precipitation amount in the double aged sample is about twice as much as in the single aged sample. Finer and more densely distributed β' phases explain why the double aged sample has higher strength and ductility than the single aged sample, which is consistent with the result from tensile tests.

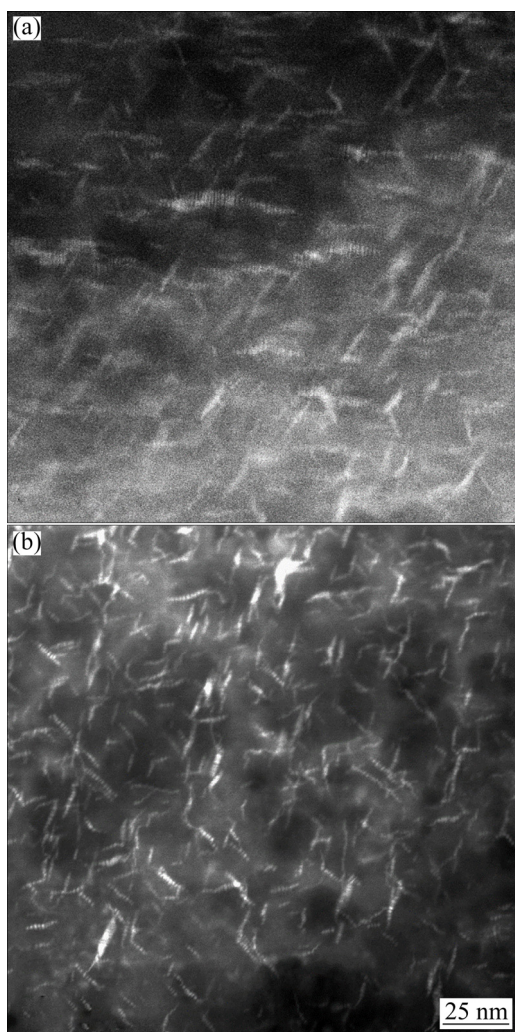


Fig. 7 HAADF-STEM images of distribution of β' phases in single aged sample (200 °C, 16 h) (a) and double aged sample (175 °C, 1 h + 225 °C, 1 h) (b)

4 Conclusions

(1) The optimum parameters of single and double aging for EV31A alloy are 200 °C, 16 h and 175 °C, 1 h + 225 °C, 1 h, which is evaluated by Vickers hardness tests and tensile tests.

(2) Compared with the traditional single aging method, double aging can reach higher UTS (from 273 to 288 MPa), higher elongation (from 4.9% to 6.6%), and lower time consumption (from 16 to 2 h), improving mechanical properties and efficiency simultaneously.

(3) The microstructure of aged EV31A is characterized, and primary Mg–RE β' phases, Mg–Zr phases, and Mg–Zn–Zr phases are observed. β' phases in EV31A alloy show similar structure with β' phases in Mg–Nd binary alloy, as well as the phenomenon of partial transformation into quasi- β_1 phases.

(4) Compared with single aged samples, finer and more densely distributed β' phases are found in double aged samples, which explains better UTS and elongation performance of double aging.

Acknowledgments

This work was supported by the National Natural Science Foundation of China (No. 51825101). Also, this work is partly supported by Xin-qiu GUO and Chong LU from Instrumental Analysis Center, Shanghai Jiao Tong University, China. The authors are grateful for their help on HAADF-STEM techniques.

References

- [1] TEKUMALLA S, SEETHARAMAN S, ALMAJID A, GUPTA M. Mechanical properties of magnesium–rare earth alloy systems: A review [J]. *Metals*, 2015, 5(1): 1–39.
- [2] CHIA T L, EASTON M A, ZHU Su-ming, GIBSON M A, BIRBILIS N, NIE Jian-feng. The effect of alloy composition on the microstructure and tensile properties of binary Mg–rare earth alloys [J]. *Intermetallics*, 2009, 17(7): 481–490.
- [3] STANFORD N, ATWELL D, BEER A, DAVIES C, BARNETT M R. Effect of microalloying with rare-earth elements on the texture of extruded magnesium-based alloys [J]. *Scripta Materialia*, 2008, 59: 772–775.
- [4] IMANDOUST A, BARRETT C D, AL-SAMMAN T, INAL K A, EL KADIRI H. A review on the effect of rare-earth elements on texture evolution during processing of magnesium alloys [J]. *Journal of Materials Science*, 2017,

- 52(1): 1–29.
- [5] ZHANG Jing-huai, LIU Shu-juan, WU Rui-zhi, HOU Le-gan, ZHANG Mi-lin. Recent developments in high-strength Mg–RE-based alloys: Focusing on Mg–Gd and Mg–Y systems [J]. *Journal of Magnesium and Alloys*, 2018, 6(3): 277–291.
- [6] ABBASI Z, EBRAHIMI R, CABRERA J M. Investigation on texture evolution and recrystallization aspects of novel Mg–Zn–Gd–Y–Nd alloys [J]. *Metals and Materials International*, 2020. <https://doi.org/10.1007/s12540-020-00729-2>
- [7] CHU Chen-liang, HU Zhi, LI Xiao, YAN Hong, WU Xiao-quan, MAI Yuan-lu. Evolution and distribution of Al₂Sm phase in as-extruded AZ61–xSm magnesium alloys during semi-solid isothermal heat-treatment [J]. *Transactions of Nonferrous Metals Society of China*, 2018, 28: 1311–1320.
- [8] NIE Jian-feng. Precipitation and hardening in magnesium alloys [J]. *Metallurgical and Materials Transactions A*, 2012, 43(11): 3891–3939.
- [9] SASAKI T, OH-ISHI K, OHKUBO T, HONO K. Effect of double aging and microalloying on the age hardening behavior of a Mg–Sn–Zn alloy [J]. *Materials Science and Engineering A*, 2011, 530: 1–8.
- [10] OH-ISHI K, HONO K, SHIN K. Effect of pre-aging and Al addition on age-hardening and microstructure in Mg–6wt.%Zn alloys [J]. *Materials Science and Engineering A*, 2008, 496: 425–433.
- [11] ZHU Shao-zhen, LUO Tian-jiao, YANG Yuan-sheng. Improving mechanical properties of age-hardenable Mg–6Zn–4Al–1Sn alloy processed by double-aging treatment [J]. *Journal of Materials Science & Technology*, 2017, 33(11): 1249–1254.
- [12] ZHANG Ding-fei, QI Fu-gang, WEI Lan, SHI Guo-liang, ZHAO Xia-bing. Effects of Ce addition on microstructure and mechanical properties of Mg–6Zn–1Mn alloy [J]. *Transactions of Nonferrous Metals Society of China*, 2011, 21: 703–710.
- [13] EMANI S, BENEDYK J, NASH P, CHEN Ding. Double aging and thermomechanical heat treatment of AA7075 aluminum alloy extrusions [J]. *Journal of Materials Science*, 2009, 44(23): 6384–6391.
- [14] IBRAHIM M, SAMUEL A, SAMUEL F. A preliminary study on optimizing the heat treatment of high strength Al–Cu–Mg–Zn alloys [J]. *Materials & Design*, 2014, 57: 342–350.
- [15] SEIDMAN D N, MARQUIS E A, DUNAND D C. Precipitation strengthening at ambient and elevated temperatures of heat-treatable Al (Sc) alloys [J]. *Acta Materialia*, 2002, 50: 4021–4035.
- [16] FAN Yun, TANG Xuan, WANG Shao-han, CHEN Bin. Comparisons of age hardening and precipitation behavior in 7075 alloy under single and double-stage aging treatments [J]. *Metals and Materials International*, 2020, <https://doi.org/10.1007/s12540-020-00875-7>.
- [17] LOPES E S M, CREMASCO A, AFONSO C R M, CARAM R. Effects of double aging heat treatment on the microstructure, Vickers hardness and elastic modulus of Ti–Nb alloys [J]. *Materials Characterization*, 2011, 62(7): 673–680.
- [18] CALIARI F R, CANDIOTO K C G, COUTO A A, NUNES C A, REIS D A P. Effect of double aging heat treatment on the short-term creep behavior of the Inconel 718 [J]. *Journal of Materials Engineering and Performance*, 2016, 25(6): 2307–2317.
- [19] LYON P, SYED I, HEANEY S. Elektron 21—An aerospace magnesium alloy for sand cast and investment cast applications [J]. *Advanced Engineering Materials*, 2007, 9(9): 793–798.
- [20] SAITO K, HIRAGA K. The structures of precipitates in an Mg–0.5at.%Nd age-hardened alloy studied by HAADF-STEM technique [J]. *Materials Transactions*, 2011, 52(10): 1860–1867.
- [21] GAO Xiang, HE Shang-ming, ZENG Xiao-qin, PENG Li-ming, DING Wen-jiang, NIE Jian-feng. Microstructure evolution in a Mg–15Gd–0.5Zr (wt.%) alloy during isothermal aging at 250 °C [J]. *Materials Science and Engineering A*, 2006, 431: 322–327.
- [22] KIELBUS A. Microstructure and mechanical properties of Elektron 21 alloy after heat treatment [J]. *Journal of Achievements in Materials and Manufacturing Engineering*, 2007, 20(1–2): 127–130.
- [23] KIELBUS A, RZYCHON T, PRZELIOR Z R. DSC and microstructural investigations of the Elektron 21 magnesium [J]. *Material Science Forum*, 2010, 638–642: 1447–1452.
- [24] RIONTINO G, LUSSANA D, MASSAZZA M, BARUCCA G, MENGUCCI P, FERRAGUT R. Structure evolution of EV31 Mg alloy [J]. *Journal of Alloys and Compounds*, 2008, 463(1–2): 200–206.
- [25] GILL L R, LORIMER G W, LYON P. The effect of zinc and gadolinium on the precipitation sequence and quench sensitivity of four Mg–Nd–Gd alloys [J]. *Advanced Engineering Materials*, 2007, 9(9): 784–792.
- [26] PIKE T, NOBLE B. The formation and structure of precipitates in a dilute magnesium–neodymium alloy [J]. *Journal of the Less Common Metals*, 1973, 30(1): 63–74.
- [27] NIE Jian-feng. Effects of precipitate shape and orientation on dispersion strengthening in magnesium alloys [J]. *Scripta Materialia*, 2003, 48(8): 1009–1015.
- [28] ISSA A, SAAL J, WOLVERTON C. Formation of high-strength β' precipitates in Mg–RE alloys: The role of the Mg/ β'' interfacial instability [J]. *Acta Materialia*, 2015, 83: 75–83.
- [29] JI Yan-zhou, ISSA A, HEO T W, SAAL J E, WOLVERTON C, CHEN Long-qing. Predicting β' precipitate morphology and evolution in Mg–RE alloys using a combination of first-principles calculations and phase-field modeling [J]. *Acta Materialia*, 2014, 76: 259–271.
- [30] TAN Jun, DONG Yu, ZHANG Hai-xiao, SUN Yong-hui, SUN Ben-zhe, QI Yang. A new insight into the beta' structure: Three categories of configurations between beta' precipitates in aged binary Mg–Nd alloy [J]. *Scripta Materialia*, 2019, 172: 130–134.

双级时效对 EV31A 合金力学性能与显微组织的影响

顾侃^{1,2}, 曾小勤^{1,2}, 陈彬¹, 王迎新^{1,2}

1. 上海交通大学 材料科学与工程学院, 上海 200240;

2. 上海交通大学 轻合金精密成型国家工程研究中心与金属基复合材料国家重点实验室, 上海 200240

摘要: 为了提升一种商用镁-稀土合金 EV31A (Mg-3Nd-1.5Gd-0.3Zn-0.5Zr) 的塑性, 探索双级时效工艺, 并且研究其对合金力学性能和显微组织的影响。在实验测得的最优双级时效参数下, 合金的抗拉强度和伸长率从单级时效的 273 MPa 和 4.9% 提升到 288 MPa 和 6.6%。双级时效的总时效时间也大幅缩短, 从 16 h 降低到 2 h。HAADF-STEM 表征发现, 合金的主要析出相 β' 相与 Mg-Nd 二元合金中的 β' 相有类似的结构, 并且双级时效使合金中的 β' 相分布更加均匀、细密, 其密度大约增至 2 倍, 而尺寸则大约减半, 这解释了合金强度和塑性提升的原因。

关键词: 镁合金; EV31A; 双级时效; 力学性能; β' 相

(Edited by Bing YANG)